Journal of Polymer Research (2023) 30:428
https://doi.org/10.1007/s10965-023-03816-1

ORIGINAL PAPER

Ultrasound assistance synthesis of optimized ion imprinted polymer for efficient and selective removal of cobalt ions from waste streams

Mahmoud Goneam Hamed[1] · **Emad Hassan Borai**[1]

Received: 26 April 2023 / Accepted: 25 October 2023 / Published online: 31 October 2023

Abstract

Selective recognition of metal ions is a real challenge for a large range of applications especially in sorption purposes. The use of ultrasound in the synthesizing and modifying of sodium alginate-based material is investigated, for enhancing the dispersion, degassing, crosslinking processes and enhance the homogeneity of ion imprinted polymer properties. Cobalt imprinted polymer was prepared using an inexpensive and simple ultrasonic-mediated polymerization process that incorporated dual functional monomers, acrylic acid, and 2-Acrylamido-2-methylpropane sulfonic acid to feature a multifunctional of carboxylic and sulfonic groups. SEM, TGA, DTA, and EDX were used to analyze the surface morphology. FT-IR study confirmed that the complexation of the Co-IIP was successfully takes place. The ability of the adsorption of ion imprinted was optimized at pH 5. The increase of the temperature from 27 to 52 °C caused the increase in the adsorption capacity. Batch tests have been performed to evaluate the selectivity mechanism, and found that the prepared polymer exhibit excellent selectivity for Cobalt, more than nickel, and strontium at 300°K (single component) were 71, 20, and 12 $mg.g^{-1}$ respectively. Pseudo-second-order kinetics and the Langmuir isotherm gave the most satisfactory explanation for the adsorption process. The prepared polymer can be reused 5 times with a very low loss in adsorption capacity. The prepared ion imprinted polymer is efficiently utilized in controlling Co^{2+} sorption/desorption processes, enabling its successful recovery from complex sample matrices for various applications especially that required separation processes.

Keywords Ultrasonic · Ionic interaction · Crown ether · Polymers · Semi-interpenetrating · Polymer network

Introduction

Cobalt is a valuable transition metal and has widespread applications in various industries, such as electronics, catalysis, and battery technology. Efficient extraction and separation of cobalt from the matrices are crucial for its effective utilization. In this regard, significant advancement in the formulation of novel analytical methods has resulted from the widespread use of chemical imprinting technology as a significant tool in the selective identification of a specific target analyte (metal ion). Ion-imprinted polymers (IPs) have undergone significant research and positive evaluations since their development [1]. Studies on ion-imprinted polymers (IIPs), in which metal ions are detected with closely related inorganic ions, are still few. The manufacture of ion-imprinted adsorbents using a distinct synthetic process was the subject of this study, as was their use in the creation of solid phase identification techniques [2]. Ultrasonic waves play a crucial role in the preparation of co-imprinted polymers (CIPs) due to their ability to enhance the efficiency of template removal, improve polymerization kinetics, and promote better imprinting effects. Ultrasound helps in facilitating the mass transfer of template molecules out of the polymer matrix, leading to increased template binding sites and higher selectivity of CIPs. Additionally, ultrasonic cavitation promotes uniform mixing of monomers, and cross-linker, resulting in well-defined polymer structures and improved rebinding properties. This technique aids in producing CIPs with enhanced recognition capabilities and greater stability for various applications, such as separation processes.

Cold water slowly dissolves sodium alginates, creating a thick, colloidal solution. Alginates are frequently utilized in the creation of suspension and emulsion as cross-linking, binding, viscosity-modifying, and stabilizing agents in a dispersed system. Alginate has a bio adhesive quality that might

✉ Mahmoud Goneam Hamed
Mahmoud_g_hamed@yahoo.com

[1] Hot Laboratories and Waste Management Center, Egyptian Atomic Energy Authority, Cairo 13759, Egypt

be advantageous in a variety of applications [3]. Studies have shown that alginate has the highest strength compared to polymers like polystyrene, chitosan, and CMC because it has been claimed that polyanion polymers are more effective in adhesive than polycation polymers or non-ionic polymers. Alginate is categorized as an anionic polymer because of its carboxyl end groups [4]. Many grades of sodium alginates produce aqueous solutions with different viscosities. Alginate solutions act as pseudo-plastic fluid and are not Newtonian because of the dispersion of chain lengths. Their lower viscosity should increase extremely quickly with dilution when dissolved in clean water. To benefit from the fusion of all distinct organic materials, sodium alginate was chemically reacted in several investigations with other organic materials with high adsorption capabilities and characterized by a variety of functional groups [5].

The creation of nanoscale materials has recently become dependent on the ultrasonic polymerization (USP) process. Greater effort is required to disperse agglomerates and resist bonding forces while processing nanomaterials. Ultrasound apparatus generally operates at frequencies in the range from kilohertz to gigahertz [6–9]. Cavitations are what lead to the desirable sonochemical effects, such as de-agglomeration, dispersion, de-agglomeration, homogenization and emulsification. H and OH radicals in high concentrations are formed in water as a result of the enhanced attractive force within the solution matrix caused by ultrasonic irradiation. Cavitation bubbles may develop later. The resulting cavitation bubble expands after absorbing gas from the matrix, collapsing at its maximum size. When a monomer's double bonds are present in or near so-called cavitation bubbles, they rupture to form radicals and start the polymerization process. In the past few decades, materials have been reported based on sodium alginate with effective heavy metal ion adsorption capabilities were created [10]. These adsorbents do, however, have several evident drawbacks, including low mechanical strength, and challenges with solid–liquid separation. To create sodium alginate-based ion imprinted polymer material with high selectivity, mechanical strength, stiffness, and porosity, the right technique of gamma radiation and ultrasonication combination must be used. In recent years, interest in using ultrasound as an external stimulus to encourage polymerization events has grown. In this edition, the basic procedures that can result in the sonolysis of a solvent or small molecule when ultrasound is used were presented [11]. Special attention is devoted to the subsequently reported systems that are controlled by techniques of reversible radical deactivation in this detailed historical survey of the progress of ultrasound-assisted radical polymerization. In the present work, the study begins by synthesizing Co-IIPs using a template polymerization technique, where cobalt ions serve as the template molecules. The resulting Co-IIPs exhibit tailored recognition sites that specifically bind to cobalt ions.

Experimental

The investigations in the ongoing study utilized deoxygenated double distilled water that would have been bubbled with pure nitrogen gas at a temperature of 80 °C as well as all reagents were of the highest purity.

Materials and methods

Sodium alginate (SA) (Analar grade). Cobalt chloride, N, N'-methylene- bis- acrylamide (MBA), and 2-Acrylamido-2-methylpropane sulfonic acid (AMPS) were used without any further purification [6, 7]. Potassium peroxodisulphate (KPS) as redox initiator and N, N, N′, N′- Tetra methylene diamine (TEMED), which was utilized as a throttle, was purchased from Aldrich. Sodium hydroxide (NaOH, micro granular pure, Poland) was employed to neutralize the acid. HCl (37%) HNO_3. The chemical compositions of IIPS were determined using IR spectra in the 400–4000 cm^{-1} range and were recorded at room temperature on an infrared spectrophotometer (Vector 22, Germany). IIPS were performed to thermo gravimetric investigations (TG-DSC 1600 °C, Caluire, France) from room temperature to 600 °C at a heating rate of 10 °C/min and in an atmosphere of argon [12]. After coating the samples with gold, the morphology of each sample was studied using a scanning electron microscope (VEGA II SEM device, Czech Republic). A computerized atomic absorption spectrometer was used to analyze metal ion concentrations.

Preparation of polymer

Cross-linking operation and chemical modification

The manufacture of sodium alginate-based adsorbents typically requires chemical modification, a combination of the high solubility and low chemical resistance, surface grafting and cross-linking are commonly used [13]. By adding particular functional groups to the surface of the adsorbents, Surface grafting can enhance metal capacity while also enhancing sorbent selectivity. Whereas cross-linking significantly boosts chemical stability and mechanical strength by fusing two or more molecules via a covalent bond. Surface grafting of functional groups onto an adsorbent can increase selectivity for specific metal ions while additionally enhancing metal absorption capacity. For the crosslinking step during preparation process of SA-*g*-P(AA-*co*-AMPS) IIPS, MBA solution (0.02 wt %) were stirred in (30 mL) of distilled water and poured dropwise into the mixture, it is sufficient for the required purpose.

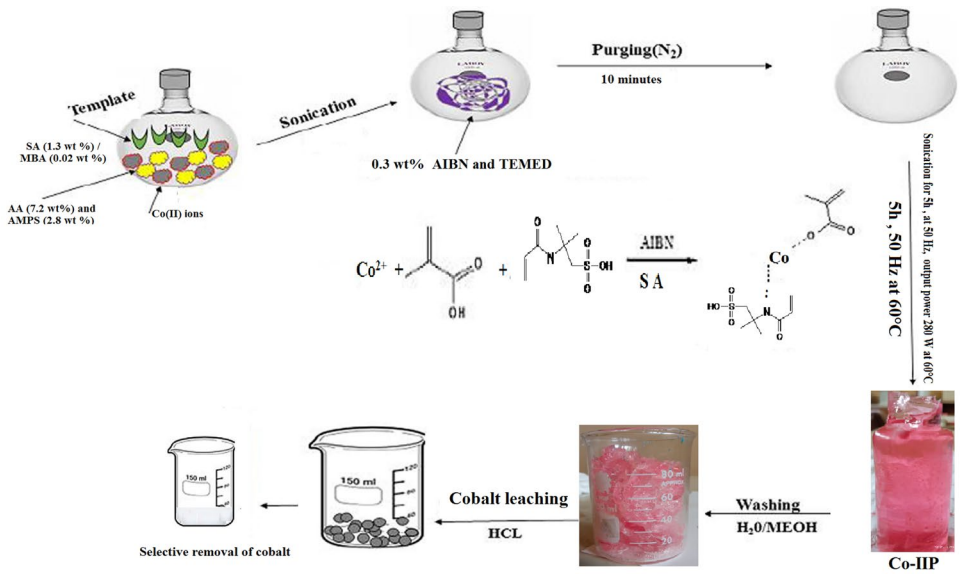

Scheme 1 Graphical representation and imprinting mechanism of Co-IIP

Synthesis of Co^{2+} ion-imprinted polymer SA-g-P(AA-co-AMPS)IIPS

The co-monomers used in the synthesis of the cobalt ion-imprinted polymer (Co-IIP) possess a strategically designed structure, incorporating essential functional groups to ensure effective cobalt ion binding and selectivity. This monomer is a multifunctional molecule, featuring, a sulfonic group, and a carboxylic group. The addition of effective co-monomers for sodium alginate is more suitable for practical applications such as the removal of heavy metals from waste streams. Sodium alginate contains -COOH and -OH groups, which helps provide the necessary binding sites for the preparation of IIPs. The first step is to attempt to build an integrated IIP entity by adding more effective monomers being more appropriate for different applications under demanding conditions, such as a wide pH and ambient temperature [6, 7]. For this purpose, the free radical polymerization technique was used to prepare Co^{2+} imprinted sodium alginate backbone SA-*g*-P(AA-*co*-AMPS)Co-IIPs according to the following procedure: a solution containing both AA (7.2 wt%) and AMPS (2.8 wt %) was stirred in 10 ml double distilled water for later use. SA (1.3 wt %) and MBA solution (0.02 wt %) were stirred in (30 mL) of distilled water and poured dropwise into the first mixture. The total mixture was put in a covered beaker and using a mechanical agitator, CoCl2 (0.3 g) dissolved in 10 ml double distilled water was added and then exposed to an ultrasonic homogenizer in the ice bath for 15 min [14]. The N2 gas was purged into the reaction for 10 min, 0.3 wt% aqueous solutions for both the redox initiator system and accelerator AIBN, and TEMED were added dropwise to the solution mixture under vigorous mechanical stirring, and N2 gas as illustrated in Scheme 1 [9].

Thereafter ultrasonic-assisted polymerization reaction was carried out for 5 h, which operates at 50 Hz with a maximum power output of 280 W at a controlled temperature of 60 °C to generate radicals [15]. The prepared IIP was washed 3 times for each acetone and double distilled water to remove unreacted materials until got a neutral pH, then dried in a vacuum oven to constant weight and put in a dryer before use. Then treated with 50 mL of 2 M HCl under continuous stirring for 3 h duration to leach out Co^{2+} ions. Thus, the imprinted cavity polymer as IIP was prepared and used to further the adsorption study. This step is to detail the specific cavity for the selective removal of Co^{2+} ions from the aqueous medium. Non-imprinted polymer (NIP) was also prepared by the same method without the use of Cobalt ions [16].

Sorption and desorption studies

For testing the sorption and selectivity of the Co-IIP to the metal ions, a series of batch adsorption experiments is performed with the Co-IIP and pairs of Ni^{3+} and Sr^{2+} were extracted by 100 mg of Co-IIP at pH 5. The percent uptake, capacity, and distribution coefficient were calculated respectively by:

$$\%\ uptake = \frac{(Ci - Ce)}{Ci} 100 \tag{1}$$

$$q(mg/g) = \frac{(C_i - C_e)V}{m} \tag{2}$$

$$K_d = \frac{C_o - C_e}{C_e} \times \frac{V}{m} \tag{3}$$

where (q) is the maximum capacity (mg/g), C_i and C_e are the initial and equilibrium concentrations (mg/L) of metal ion, respectively, m is the mass of the adsorbent used (g), and V is the initial volume of the aqueous solution (L). Weight to

volume ratios was studied by varying the volume from (0.01. 0.05 to 0.1) litter. Batch investigations were used for the desorption of Co^{2+} ions onto the prepared (Co-IIP), in which cobalt ions were pre-concentrated onto imprinted polymer material (IIP) and eluted by 20 mL of 2 M HCl solution at about 3 h stirring time. After filtering the ultimate solution, containing Co^{2+} ions has been obtained from the Co-IIP [17]. The cobalt concentrations regarding the solutions were then determined, and the percentage of sorbed metal ions was calculated using Eq. (4) and represented as the amount of metal extraction desorption %.

$$D\% = \frac{C_a}{C_s} \times 100 \tag{4}$$

C_a is the ions concentration in the aqueous phase and C_s is the concentration in the solid phase which can be calculated from the difference between the initial and final concentrations (C_o—C_e).

Results and discussion

Characterization of the prepared adsorbents

FTIR analysis

According to the synthesized polymer's FTIR spectroscopy results, which are depicted in Fig. 1, hydrogen bonds are generated between the (SA) network and the linear reactive monomers AA-co-AMPS [6, 7]. The stretching of a C-H that is overlapping with a carboxylic acid's OH is responsible for the wide band at 3354 cm^{-1}. The existence of a stretching band of C = O corresponding to carboxylic acid is demonstrated through the absorption band at 1680 cm^{-1} [4]. The presence of a characteristic band of stretching NH_2, at 3208 cm^{-1}, and 1426 cm^{-1} characteristic of primary amides. The sulfonic acid (SO_3) is asymmetric, and symmetric at 1245 and 1076 cm^{-1} respectively [18].

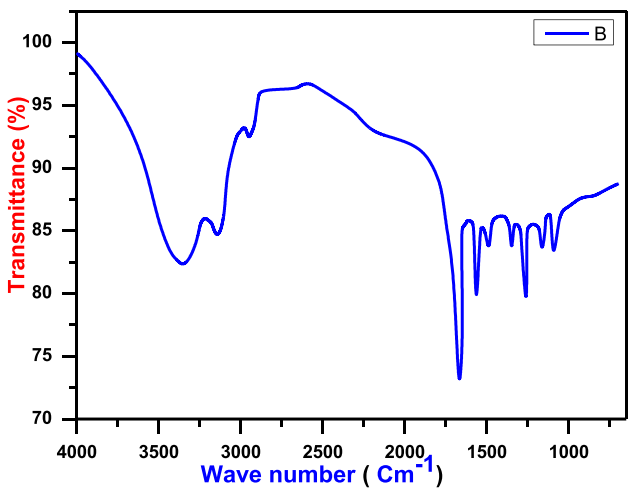

Fig. 1 FTIR spectrum of the co-ion imprinted polymer SA-*g*-P(AA-*co*-AMPS), without template cobalt ions

Scanning electron microscope (SEM)

SEM analysis is conducted to examine the surface morphology of non-imprinted (NIP), co (II) imprinted (Co-IIP), and leaching IIP prepared by ultrasonic homogenizer under optimum conditions as shown in Fig. 2, it was reported that NIP's surface varied from Co-IIP and leached polymer surfaces [14]. The morphologies of the prepared polymers are typically uniform in shape without agglomeration, indicating the high efficiency of the ultrasonic effects on the final product Fig. 2(a) represents NIP, which shows that small particles with smooth surface, the image revealed an irregular shape with a rough surface possibly due to the processes of crosslinking and grafting [19]. Figure 2(b), represents "Co-IIP," and depicts the IIP's morphological analysis, the surface becomes rougher, making unique recognition sites that are comparable in size and shape in the polymeric matrix and the roughness increased. The cobalt ion, which is released from the voids in the polymer matrix [9]. The SEM images showed that metal template ions affected by absence, and presence, of co ions inside the polymer matrix were the major causes of the morphological variations in the polymer synthesis.

Thermogravimetric analysis (TGA)

An alternative kinetic model of the prepared polymer degradation was created using thermogravimetric analysis (TGA) and differential thermal analysis (DTA), as illustrated in Fig. 3. 10 °C/min of heat was applied to the produced polymer. The decomposition occurs in three stages, the first of which occurs between (27 and 200 °C) and has an endothermic peak at 149 °C and a loss weight of 5.66%. This weight loss may be caused by the removal of all surface and matrix-bound moisture in addition to any absorption or coordinated molecules of water out from the polymer. A weight loss of 35.2% is seen in the second stage from (201 to 304 °C), which exhibits endothermic maxima at 255 °C, as a result of CO_2 release brought on by the dehydration of acrylic acid. The third stage from (304 to 552 °C), with a maximal endothermic peak at 516 °C, exhibits a considerable weight loss that ranges from 36.45%, which may be caused by the elimination of volatile hydrocarbon produced in the oxide state and small chain fragments made by chain scission. The process preceding the main chain scission and

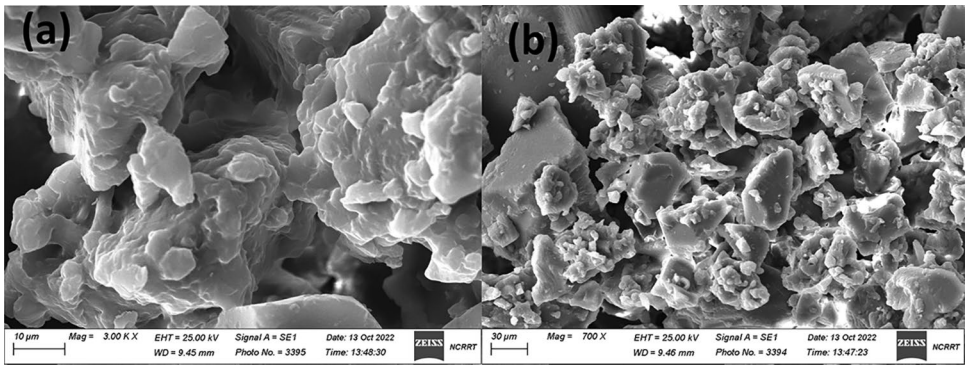

Fig. 2 **a** and **b**: SEM micrographs of non-imprinted (NIP) and SA-*g*-P(AA-*co*-AMPS)IIPS respectively

full degradation to the oxide state is what causes a weight loss of 6.4% in the fourth stage from (552 to 700 °C) and an overall weight loss of 83.72% [5].

Energy dispersive x-ray (EDX) and mapping spectra

The Energy Dispersive X-ray (EDX) analysis is a form of elemental analysis related to electron microscopy that relies on the production of distinctive X-rays to identify the elements contained in the prepared materials. Both semi-qualitative and semi-quantitative data are present at various Levels in the EDX analysis spectrum. As the objective is to determine if a metal ion is present or absent in a polymer matrix. By the examination of cobalt imprinted, non-imprinted, and leached polymers, EDX spectroscopic analysis was found to be quite effective. Three peaks at various Kevs are visible in the EDX spectrum of IIP, as illustrated in Fig. 4(a). The peaks were verified by comparing the Kev to be carbon, oxygen, nitrogen, and cobalt. Cobalt ions have an additional peak in the IIP spectrum, which supports the successful imprinting of the Co^{2+} template ion. Our mapping demonstrated that the Co(II) ions were initially present both at the surface and in the core, but at a somewhat lower concentration. The spectrum in Fig. 2(b) shows that the template is completely removed from the polymer matrix after treatment with acid. The morphology demonstrates that template cobalt ions are leached, leaving behind significant voids that are comparable in size and shape to the template species, increasing the produced polymer's effectiveness towards divalent ions in general and the cobalt ions in particular [16].

Applicability of polymeric resin for sorption of some metal ions

Optimizing weight to volume ratio for efficient adsorption

Theses process is acritical factor to control in sorption process and consume the polymer loss for over using dosage, which involves analyzing the mass of the imprinting polymer in relation to its volume. It is a crucial aspect to understand the polymer properties, efficiency of binding, capacity and applications. A higher weight to volume ratio allows for more binding sites and a greater capacity to capture target ions, enhancing the ion imprinting polymer performance in the selective sorption processes. Figure 5 illustrates that the sorption efficiency and selectivity of IIP for Co^{2+} increases as V/m increases over the other investigated divalent Ni^{2+} and Sr^{2+} ions.

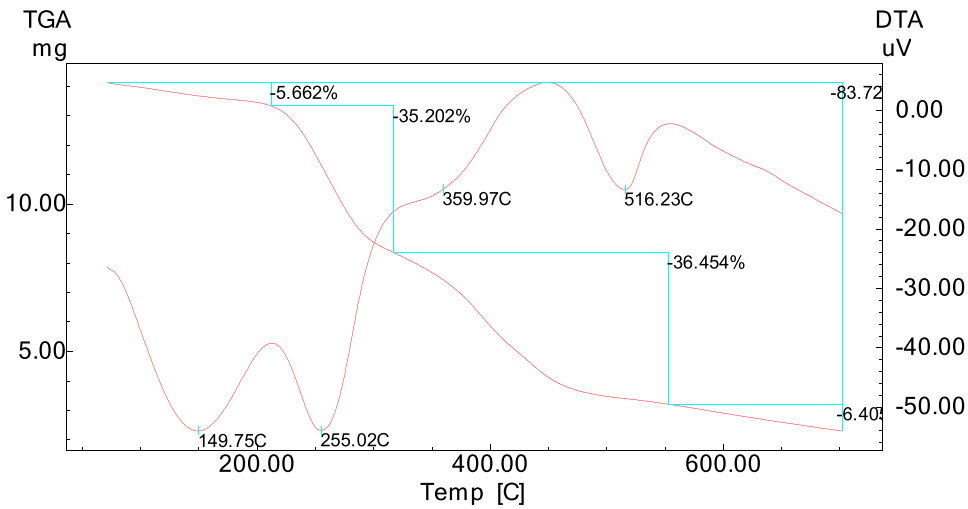

Fig. 3 DTA and TGA curves for polymer

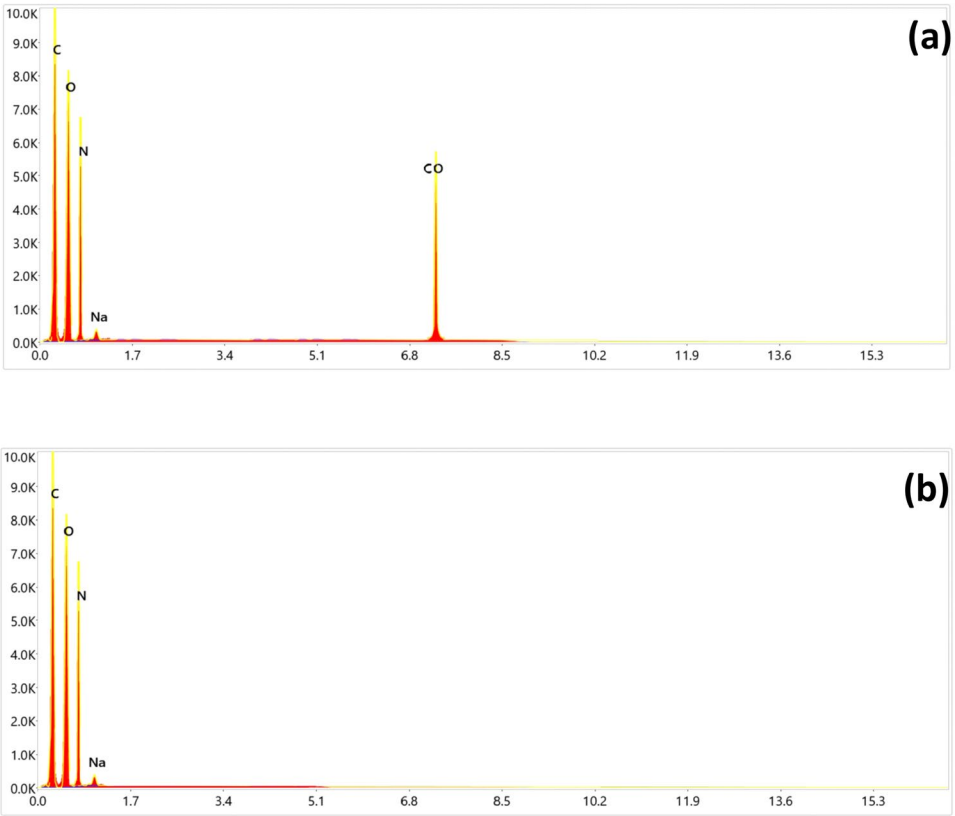

Fig. 4 **a**, **b** The EDX image of Co(II) imprinted and leached imprinted polymer, respectively

Effect of contact time on metal sorption

A batch equilibration approach has been used to study the percent uptake of the synthesized IIP towards the ions Co^{2+}, Ni^{2+}, and Sr^{2+} individually as a function of time. According to (Fig. 6), as the function of time before equilibrium grew, the percentage of IIP uptake also increased. The highest percentage uptake for the examined ions was reached after 2.0 h [20]. The order of the highest sorption uptake has always been $Co^{2+} > Ni^{2+} > Sr^{2+}$ ions. The high percent uptake (94%) for Co^{2+} may be attributed to the pores size made specifically for the cobalt ions in the IIP as a result of the entrance

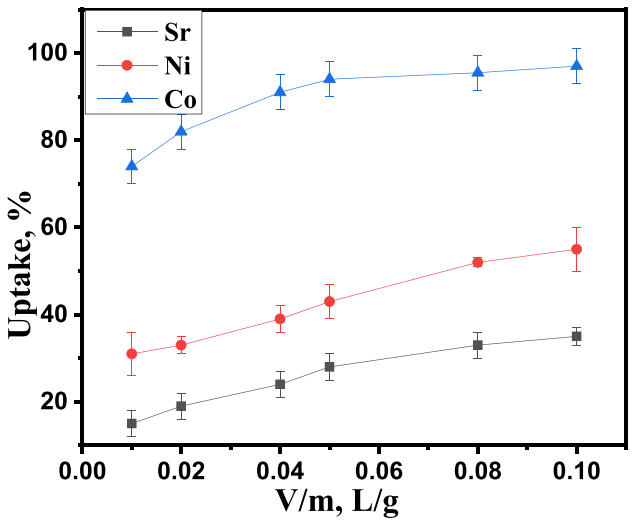

Fig. 5 Effect of different V/m ratios in L/g of IIP on sorption of Co^{2+}, Ni^{2+}, and Sr^{2+} ions

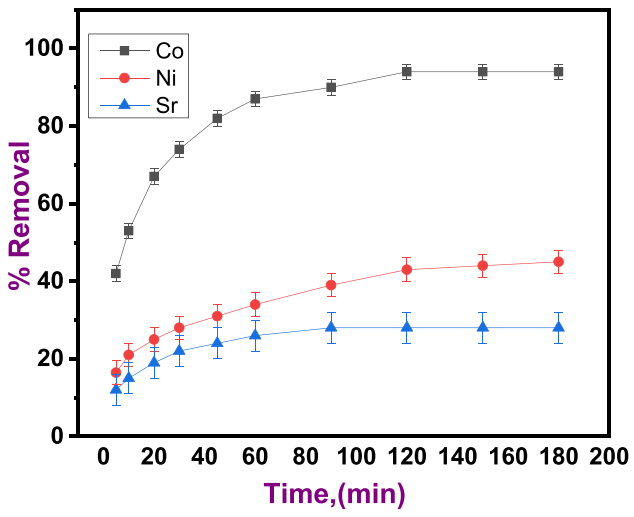

Fig. 6 Effect of time on the percent uptake of IIP (0.05 g resin, 10 ml, pH = 4.0 at 300°K)

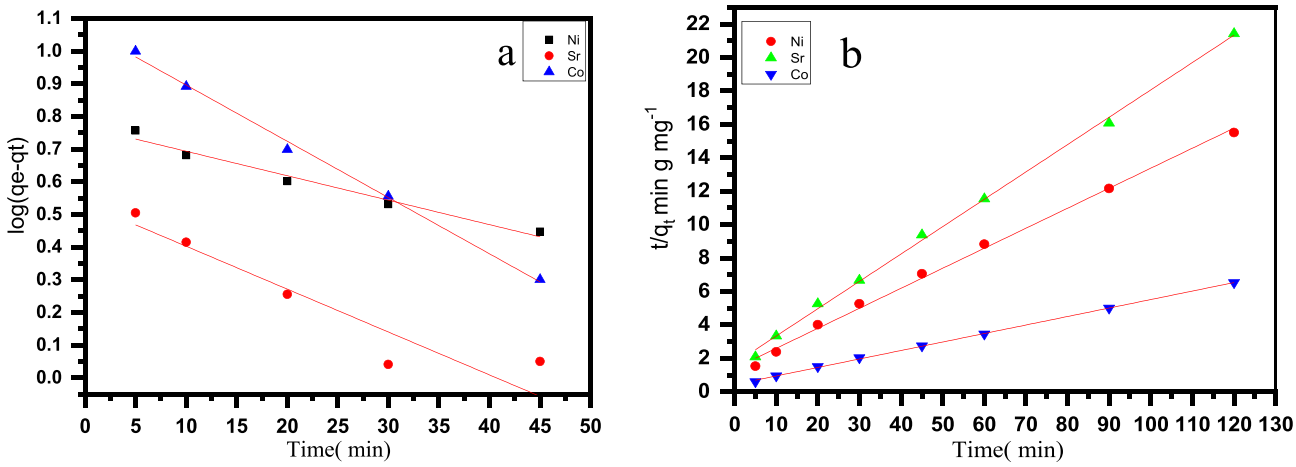

Fig. 7 Shows the pseudo-first- (**a**) and pseudo-second-order, (**b**) kinetics for sorption of Co^{2+}, Ni^{2+}, Sr^{2+} ions. Experimental conditions: time (5–120 min), concentration of Co^{2+}, Ni^{2+}, Sr^{2+} ions (100 mg/L), temp 300 °C, pH 4

and leaching of the cobalt ion In addition to the active sites specific for cobalt ions that are visible owing to IIPs. On the other hand, the maximum percent uptake of Ni^{2+} and Sr^{2+} ions decreases to 45, and 27% which, illustrates the benefits of ion imprinted polymer and reflects a convenient uptake percent for cobalt ions.

The time needed to reach the adsorption equilibrium is essential to the adsorption process [21]. Thus, two adsorption kinetics models were employed to assess the data and determine the equilibrium time. The pseudo-first-order (5) and pseudo-second-order (5) kinetics equations are given below:

$$\log(q_e - q_t) = \log q_e - \frac{K_1}{2.303}t \tag{5}$$

where q_e denotes the adsorption capacity and qt represents the adsorption capacity at the time (t) to reach equilibrium, whereas k_1 denotes the adsorption rate constant. q_t is adsorption capacity mg/g at a time (t) and k_2 represents the rate constant for pseudo-second-order Kinetics [22].

$$\frac{t}{q_t} = \frac{1}{K_2 q_e^2} + \frac{1}{q_e}t \tag{6}$$

Comparing the regression coefficient values (R^2) of the pseudo-first- and second-order kinetics, as depicted in Fig. 7(a and b), respectively, it was found the pseudo-second-order has the highest R^2 values, as listed in Table 1.

Furthermore, the experimental and computed values of the amount sorbed are more similar.

The Elovich model has been widely used to analyze chemisorption kinetic data and is often valid for systems in which assuming that actual decent surfaces have kinetic heterogeneity [6, 7]. Elovich parameters and the correlation coefficient (R^2) values of fitting this model were calculated from the slope and intercept of the plots of q_t versus ln(t) (Fig. 8), and were showed in Table 2. This model can be expressed as follows:

$$q_t = \frac{1}{\beta}\ln(\alpha\beta) + \frac{1}{\beta}\ln(t) \tag{7}$$

where q_e = amount of adsorbate adsorbed at equilibrium (mg/g). β is the desorption constant ($g.mg^{-1}$) during any experiment. α = Initial adsorption rate (mg. g^{-1} min^{-1}) The kinetic plots of q_t versus t for studied ions sorption gives a linear relationship. The high correlation coefficient (r^2) shows the success of the elovich model. This obtained data declared that the obtained results from the elovich equation are not fit well with the experimental data with low correlation coefficients (R^2).

The prediction of the rate-limiting stage is a critical aspect in the adsorption mechanism. The adsorption process governs it, which is often necessary for the design mechanism. Solute transfer in a solid–liquid sorption process is often characterized by extrinsic mass transfer (boundary

Table 1 Kinetic parameters of pseudo-first- and pseudo second- order for the sorption of Co^{2+}, Ni^{2+}, Sr^{2+} ions

Ions	$q_{e,\,exp}$	First-order model			Second-order model		
	(mgg^{-1})	$K_1(min^{-1})$	q_1(mg/g)	R^2	K_2(g/ mg.min)	q_2(mg/g)	R^2
Co^{2+}	18.8	-0.039	2.932	0.997	0.006	20.000	0.999
Ni^{2+}	9.0	-0.013	2.098	0.990	0.009	8.620	0.992
Sr^{2+}	5.6	-0.041	1.823	0.995	0.015	6.134	0.998

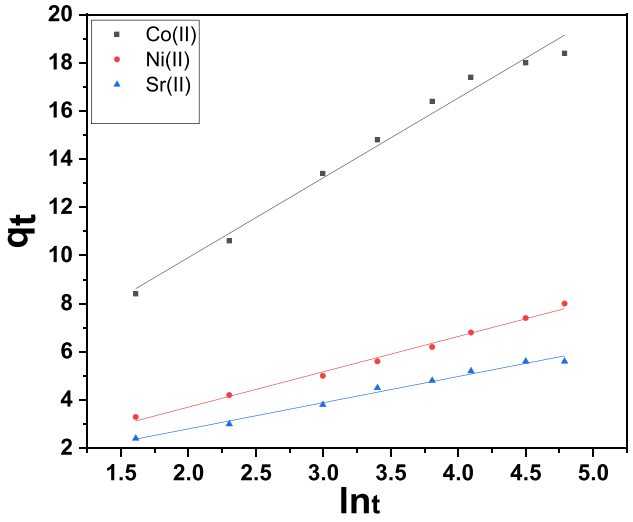

Fig. 8 Elovich plots for sorption of Co^{2+}, Ni^{2+}, and Sr^{2+} ions sorbed onto ion-imprinted Polymer

layer diffusion), intraparticle diffusion, or both. Fitting an intraparticle diffusion plot is the most often used approach for determining the mechanism involved in the adsorption process [23]. According to Weber and Morris, an intraparticle diffusion coefficient K_{int} is given by the equation

$$q_t = K_{ad} t^{\frac{1}{2}} + C \quad (8)$$

where K_{int} is the intra-particle diffusion rate constant (mg g^{-1} $min^{-0.5}$). The plot of qt versus $t^{0.5}$ at different initial solution concentrations gives the value of K_{int} and may present multi-linearity which indicates two or more steps occurring in the adsorption process. The external surface adsorption or immediate adsorption stage is takes place firstly. The second is the progressive adsorption stage when the intraparticle diffusion rate is regulated. The third stage is the ultimate equilibrium stage, in which intraparticle diffusion decreases due to the extremely low solute concentration in the solution. Table 3 shows the computed parameters. The intraparticle diffusion rate was determined from the slope of the gentle-sloped region. K_{int} values were greater at higher concentrations. The best fitting attained for the testing data with high regression coefficient values, suggest that intraparticle

Table 2 Kinetic parameters of the Elovich model for the sorption of studied ions

Ion	$q_{e,\,exp}$ (mg g^{-1})	β (g mg^{-1})	α (mgg^{-1} min^{-1})	R^2
Co^{2+}	18.8	0.30	9.04	0.99
Ni^{2+}	9.0	0.68	2.47	0.98
Sr^{2+}	5.6	0.92	1.91	0.98

Table 3 Kinetic parameters of the IPD model for the sorption of studied ions

Ion	$q_{e,\,exp}$ (mgg^{-1})	Intra-particle diffusion equation		
		K_{ad} (mgg^{-1} $min^{-1/2}$)	C (mg g^{-1})	R^2
Co^{2+}	18.8	1.43	8.21	0.91
Ni^{2+}	9.0	0.65	2.86	0.99
Sr^{2+}	5.6	0.47	2.22	0.93

diffusion may play a substantial role in metal adsorption onto adsorbent, as illustrated in Fig. 9.

Effect of pH on sorption behavior

The solution's pH level plays an important role in influencing the adsorption behavior. Figure 10 depicts a typical relationship between metal ion uptake and solution pH. The sorption capacity of IIP increased as the pH value raised from 1.0 to 5.0 and showed up at 18.8, 9.0, and 5.6 mg g^{-1} at pH 5.0 related to 94, 45, and 38 removal % for the studied metal ions Co^{2+}, Ni^{2+}, and Sr^{2+} respectively. This can be explained by the presence of a large number of hydroxyl, carboxyl and sulfonic function groups in the structure of the IIP, which, can dissociate to form carboxylate ion at higher pH, besides to the effect of specific recognition sites made specific for Co(II) ions. Even so, metal hydrolysis will occur at pH values greater than 5.0. Meanwhile, with low pH levels, the competing sorption of H^+ and metal ions on the same effective sorption site reduces metal uptake [19]. Significant change in selectivity of IIPs towards Co^{2+} ions was observed as a function of increasing pH due to procedures used in the preparation process to increase the sorption of Co^{2+} ions in the specially designated Co^{2+}

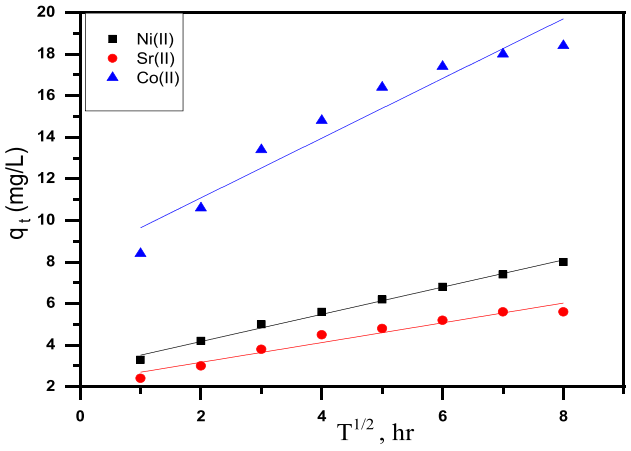

Fig. 9 Morris–Weber kinetic graphs of Co^{2+}, Ni^{2+}, and Sr^{2+} ions sorption on the IIP

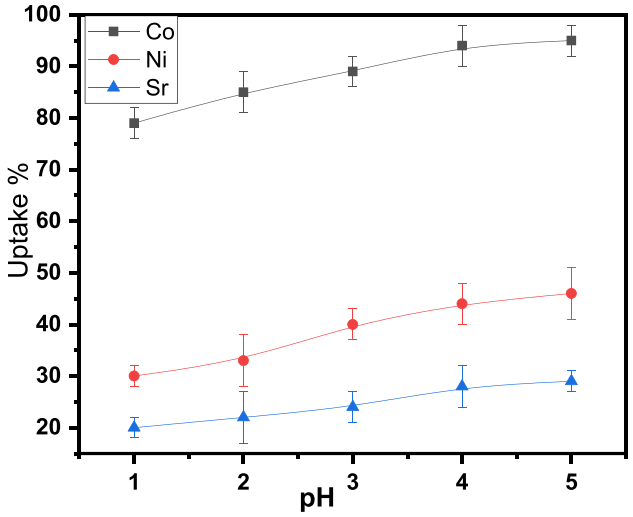

Fig. 10 Effect of pH on the sorption of resin (0.05 g resin, 10 ml and time = 2 h's at 300°K)

cavities, resulting in significant selectivity of the prepared IIPS towards Co^{2+} ions at pH 5.0.

Effect of initial metal ions concentration and sorption isotherms

The interaction of Co^{2+}, Ni^{2+}, and Sr^{2+} ions with the synthesized sorbent has valuable implications for identifying the sorption mechanism [24]. The species of Co^{2+}, Ni^{2+}, and Sr^{2+} ions on IIP surfaces are influenced not only by adsorbent characteristics, but additionally by the structure of ionized species generated at different pH levels. The influence of metal ion concentration on the adsorption capacities of the prepared IIP for Co^{2+}, Ni^{2+}, and Sr^{2+} ions on to the polymer surfaces with specific recognition sites has been studied at pH 5.0 to mitigate metal hydrolysis, in the range of 50 to 500 mg L^{-1} at different temperatures, as shown in Fig. 11. The resulting findings indicate that the maximal sorption capacity for Co^{2+}, Ni^{2+}, and Sr^{2+} ions at 300 K^o was 71, 20, and 12 mg/g, respectively. As shown in Table 4, their sorption capabilities are significantly high when compared to other ion imprinted chemical sorbents.

Sorption equilibrium is usually described by an isotherm equation whose parameters express the surface properties and affinity of the prepared SA-*g*-P(AA-*co*-AMPS)IIPS. The association between the quantity of adsorbate on the adsorbent and the concentration of dissolved adsorbate in the liquid at equilibrium is described by an adsorption isotherm. Throughout this study, the sorption isotherms for the removal of Co^{2+}, Ni^{2+}, and Sr^{2+} onto IIP at three distinct temperatures (300, 315, and 325) were investigated.

Figure 11 showed that the quantity sorbed on IIP increased with increasing temperatures for all ions, indicating that the process appeared endothermic. Langmuir and Freundlich created models that are frequently was using to interpret experimental isotherm results. These equilibrium models' equation parameters and accompanying thermodynamic assumptions frequently give some insight into the sorption mechanism and the surface attributes. The magnitude of the correlation coefficient (R^2) for the linear regression was often used to evaluate the correctness of an isotherm model's fit to experimental equilibrium data, i.e., the isotherm with the closest R^2 value to unity was regarded to give the best fit.

Sorption isotherm

Langmuir isotherm model

The Langmuir sorption isotherm model, represented in Fig. 12, which is predicated on idealized monolayer adsorption of the sorption surfaces, is deceptive for most real sorption systems that include fundamentally high porosity and functionally diverse chemicals [25]. Equation (9) provides the linear version of the Langmuir equation:

$$\frac{C_e}{q_e} = \frac{1}{Q_o b} + \frac{1}{Q_o} C_e \tag{9}$$

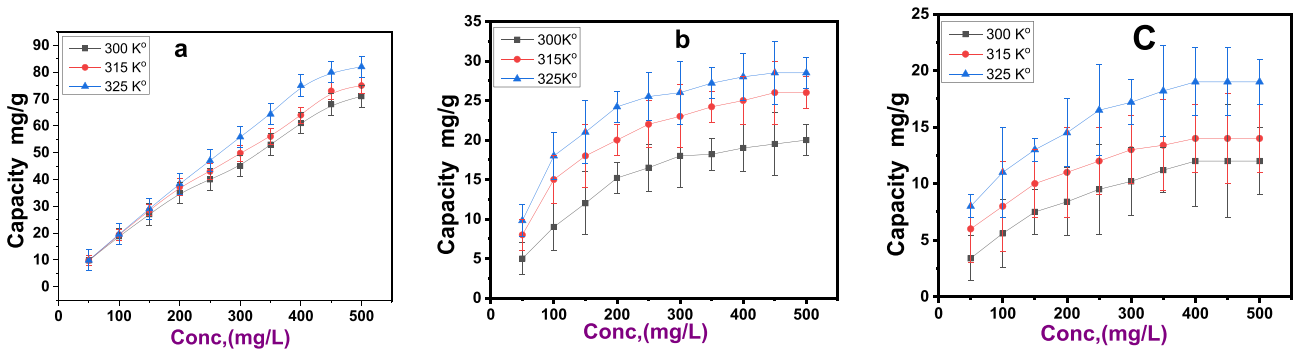

Fig. 11 Effect of initial metal ion concentration at different temperature for **a** Co^{2+}, **b** Ni^{2+}, and **c** Sr^{2+} ions onto (0.05 g resin, 10 ml and time = 2 h's at pH = 5) and different temperatures (300, 315 and 325) °K

Table 4 Langmuir and Freundlich isotherm parameters for the sorption of Co^{2+}, Ni^{2+}, and Sr^{2+} ions onto IIP

Ions	Temperature (K)	Langmuir model parameter				Freundlich model parameter		
		Q^o (mg/g)	b (L/mg)	R^2	R_L	K_f (mg/g) $^{1/n}$	n	R^2
Co^{2+}	300	63.2	0.06	0.98	0.02	2.77	2.49	0.97
	315	66.7	0.10	0.98	0.01	2.86	2.42	0.97
	325	71.4	0.16	0.98	0.01	2.69	2.25	0.96
Ni^{2+}	300	25.64	0.01	0.99	0.11	1.95	4.07	0.95
	315	27.02	0.03	0.98	0.03	2.21	4.1	0.98
	325	28.57	0.10	0.98	0.01	2.34	4.18	0.96
Sr^{2+}	300	16.39	0.01	0.98	0.14	0.99	2.34	0.97
	315	15.87	0.01	0.98	0.06	1.08	2.49	0.97
	325	20.83	0.02	0.98	0.04	1.22	2.74	0.97

where Q^o, the monolayer capacity of the adsorbent (mg/g), b Langmuir constant (L/mg) and related to the free energy of sorption, q_e theoretical saturation capacity (mg/g). The graphic presentations of (C_e/q_e) versus C_e give straight lines studied of ions sorbed onto IIP.

The numerical value of constants Qo and b evaluated from the slope and intercept of each plot are given in Table 4. The value of saturation capacity Qo corresponds to the monolayer coverage and defines the total capacity of the adsorbent for a specific metal ion.

One of the essential characteristics of the Langmuir model could be expressed by a dimensionless constant called equilibrium parameters RL

$$R_L = \frac{1}{1 + bC_o} \tag{10}$$

where C_o is the highest initial ion concentration (mg/L). The value of RL indicates the type of isotherm to be irreversible (RL = 0), favorable (0 < RL < 1), linear (RL = 1), or unfavorable (RL > 1). All the RL values (Table 4) were found to be less than 1 and greater than 0 indicating the favorable sorption isotherms of ions.

Table 4 shows that the monolayer sorption capacity (Qo) values of produced IIPs towards Co^{2+} ions are greater than those of Ni^{2+} and Sr^{2+} ions. The Langmuir constants Qo and b values for all ion sorption increased with temperature. The rise in sorption capacity with temperature indicated that the active surface accessible for sorption increased with temperature.

Freundlich isotherm model

Freundlich equation is derived to model the multilayer sorption and for the sorption on heterogeneous surfaces [26]. The logarithmic form of the Freundlich equation is written as:

$$\log q_e = \log K_f + (1/n) \log C_e \tag{11}$$

where K_f is the constant indicative of the relative sorption capacity of polymer (mg/g) and 1/n is the constant indicative of the intensity of the sorption process. Figure 13 displays a graphic display of log qe vs log Ce, indicating that the sorption of investigated ions obeys the Freundlich isotherm throughout the entirety of the range of sorption concentration investigated. Table 4 also provides the quantitative data of the constants 1/n and Kf, which are obtained from the slope and intercepts that used a linear regression fitting methodology. These findings indicate that the Freundlich intensity constant (n) for the ions studied is greater than unity. This has physical implications for the essential features of isotherms in addition to the interaction between

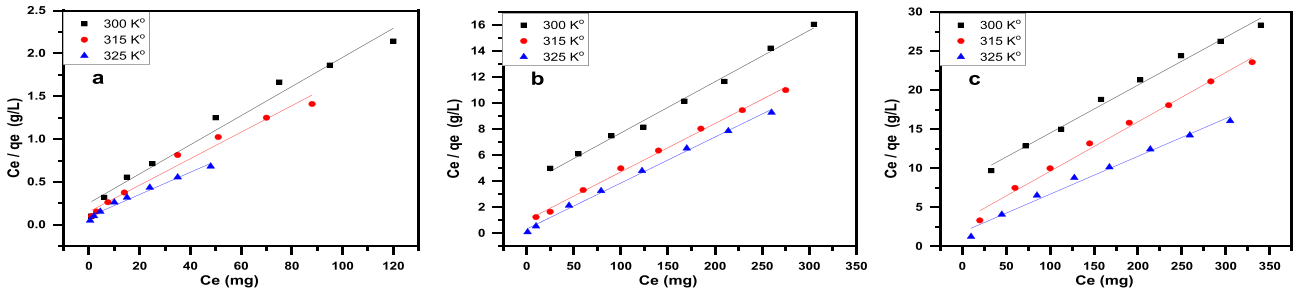

Fig. 12 Langmuir isotherm plots for the sorption of **a** Co^{2+}, **b** Ni^{2+}, and **c** Sr^{2+} ions sorbed onto IIPs at different Temperatures

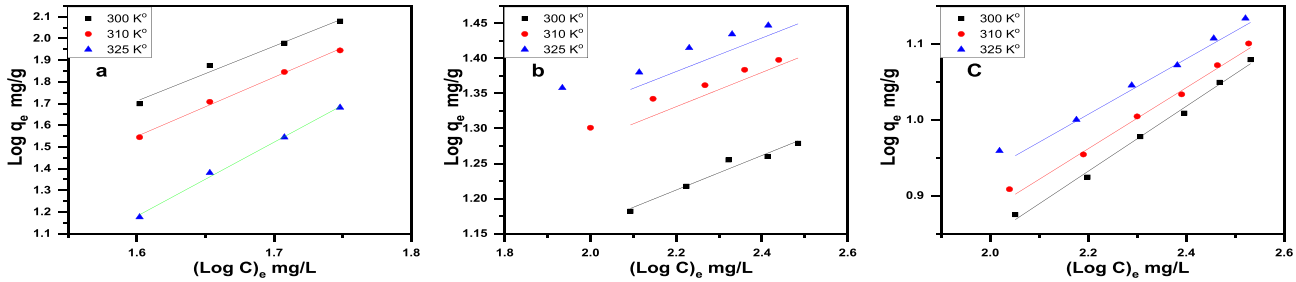

Fig. 13 Freundlich isotherm plots for the sorption of Co^{2+}, Ni^{2+}, and Sr^{2+} ions sorbed onto IIP

species and polymer. In this circumstance, n > 1 for all ion species, polymeric samples showed a rising sorption tendency to rising solid phase saturation. The reason is that as just the surface coverage of the adsorbent increases, the forces of attraction between the ions species, such Vander Waals forces, rise exponentially than the repulsive forces, evidenced by short-range electronic or long-range Coulombic dipole repulsion (electrostatic force), which means that the ions have a greater propensity to bind to the IIP.

Regeneration and reusability of Co-IIP

The reusability and chemical stability of (Co-IIPS) are essential features in actual application. As shown in Fig. 14, a total of five adsorption–desorption experiments were conducted to examine the adsorption and chemical changes of IIPs. 100 mg of Co-IIP was used in the adsorption–desorption cycle 5 times under optimal conditions to evaluate its reusability, as shown in Fig. 14. The adsorption–desorption experiments were conducted with no notable change in adsorption capacity, which is a crucial characteristic from a financial perspective. Studies indicate that the Co-IIP can be reused in 5 adsorption–desorption cycles with no recognized change in the sorption capacity. As a result of using the prepared Co-IIP 5 times, adsorption capacity is reduced by about 9%.

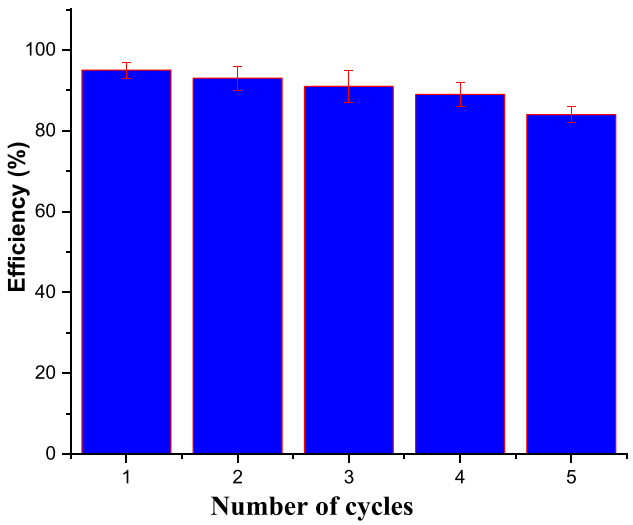

Fig. 14 Reusability studies of the Co-IIP in several cycles of efficiency

Effect of interfering ions on IIP efficiency

The study explores potential trials to mitigate the effect of interfering ions. To assess the impact of interfering ions, a series of experiments are conducted using synthetic solutions containing cobalt ions along with different concentrations of interfering ions. These interfering ions include represented heavy metal (pb^{2+}) and common major ions (K^+, Na^+, Mg^{2+}, and Ca^{2+}) found in environmental or industrial samples. The extraction efficiency and selectivity of Co-IIPs are evaluated un various conditions. To verify this assumption, solutions containing 0.1 $g.L^{-1}$ of Co^{2+} ions and coexisting ions (K^+, Na^+, Mg^{2+}, Ca^{2+} and pb^{2+}) were prepared as multicomponent system. The results illustrated in Table 5 shows that, monovalent ions have a negligible effect (Na^+, K^+), while others divalent ions (Mg^{2+}, Ca^{2+} and pb^{2+}) have more significant effect that hinder cobalt sorption (less than 10%). The findings reveal that certain interfering ions can compete with cobalt ions for binding sites on the Co-IIPs, leading to reduced extraction efficiency and selectivity but in a very small percentage, which shows the efficiency of the prepared IIPS in selective sorption of cobalt ions.

Table 5 Effect of the interfering ions on the recovery of cobalt ions

.Interfering Ion	Interfering Ion concentration	Co^{2+} Recovery
K^+	100 mg/l	94.0
Na^+	100 mg/l	93.4
Mg^{2+}	100 mg/l	82.2
Ca^{2+}	100 mg/l	80.0
pb^{2+}	100 mg/l	91.0

Table 6 Comparison between Co-IIPs and other adsorbents for Cobalt adsorption

Adsorbents	q_e of Co^{2+} (mg/g)	Ions	Refs
Al-pillared bentonite clay	30.53	cobalt(II)	[27]
lemon peel as biosorbent	49.80	cobalt(II)	[28]
extracellular polymeric substances	50	cobalt(II)	[29]
Co-IIPs	71	cobalt(II)	**Our work**

Comparison with other adsorbents for the removal of Co^{2+}

Table 6 summarizes the selective sorption of Co-IIPS as compared to other adsorbents reported in the literature. It could be observed that Co-IIPS had a significant higher sorption capacity and selectivity for Co^{2+} ions. By adding particular functional groups specially present on the surface of the adsorbents, surface grafting can increase the metal capacity and improve the selectivity of the IIP. Several investigations have shown that hydroxyl, carboxyl, and sulfonate groups are quite effective at binding metal ions. The sulfonic group's (SO_3H) polar nature enhances the affinity of binding cobalt ions to the polymer, through strong electrostatic interactions. The carboxylic group (COOH) can participate in ion coordination and contribute to the overall stability of the cobalt ion binding sites, and enhances the polymer capacity. By incorporating these functional groups, the monomer offers a synergistic effect, enabling the cobalt ion-imprinted polymer to exhibit high selectivity and affinity for cobalt ions. Whereas cross-linking significantly boosts chemical stability and mechanical strength by fusing two or more molecules via a covalent bond.

Conclusion

Ultrasound technique is used to nebulize solutions into tiny mists, which enhances the generation of radical species that can be incorporated into chain-growth radical polymerizations. In this study, SA-g-P(AA-co-AMPS) ion imprinted polymer was effectively prepared using the ion-imprinting method and ultrasonic homogenizer. The prepared polymer exhibits excellent selectivity for cobalt, more than nickel, and strontium, in addition to relative high sorption capacities 71, 20, and 12 mg.g^{-1}, respectively. The adsorption isotherms could be well fitted by the Langmuir equation. The adsorption capacity of CO-IIPs is higher than that presented in the literature. The adsorption process could be best described by the second-order equation. The results suggest that the adsorption behavior of Co^{2+} ions on IIPs was mainly affected by chemical interaction rather than physical process. It can be concluded that IIPs is a promising adsorbents for the selective of cobalt ions.**Funding** Open access funding provided by The Science, Technology & Innovation Funding Authority (STDF) in cooperation with The Egyptian Knowledge Bank (EKB).

Data availability The data that support the findings of this study are available on request from the corresponding author.

Declarations

Competing interest The authors declare that they have no known competing financial interests or personal relationships that could have appeared to influence the work reported in this paper. The authors declare the following financial interests/personal relationships which may be considered as potential competing interest.

References

1. Kusumkar VV, Galamboš M, Viglašová E, Daňo M, Šmelková J (2021) Ion-imprinted polymers: Synthesis, characterization, and adsorption of radionuclides. Materials. https://doi.org/10.3390/ma14051083
2. Kakavandi MG, Behbahani M, Omidi F (2017) Application of ultrasonic assisted-dispersive solid phase extraction based on ion-imprinted polymer nanoparticles for preconcentration and trace determination of lead ions in food and water samples. Food Anal Methods. https://doi.org/10.1007/s12161-016-0788-8
3. Khalil M, Dakroury GARS, Borai EH (2022) Efficient sorption and group separation of rare earth elements using modified CuO nanocomposite. Surf Interfaces 33. https://doi.org/10.1016/j.surfin.2022.102233
4. Fujisawa S, Kaku Y, Kimura S, Saito T (2020) Magnetically collectable nanocellulose-coated polymer microparticles by emulsion templating. Langmuir 36(31). https://doi.org/10.1021/acs.langmuir.0c01533
5. Hong RY, Feng B, Liu G, Wang S, Li HZ, Ding JM, Zheng Y, Wei DG (2009) Preparation and characterization of Fe3O4/polystyrene composite particles via inverse emulsion polymerization. J Alloy Compd. https://doi.org/10.1016/j.jallcom.2008.09.060
6. Borai EH, Hamed MG, El-kamash AM, Siyam T, El-Sayed GO (2015) Template polymerization synthesis of hydrogel and silica composite for sorption of some rare earth elements. J Colloid Interface Sci 456. https://doi.org/10.1016/j.jcis.2015.06.020
7. Borai EH, Hamed MG, El-Kamash AM, Siyam T, El-Sayed GO (2015) Synthesis, characterization and application of a modified acrylamide-styrene sulfonate resin and a composite for sorption of some rare earth elements. New J Chem. https://doi.org/10.1039/c5nj01479d
8. El-kamash AM, Borai EH, Hamed MG, Abo-Aly MM (2019) Fixed bed sorption studies on the removal of uranium and gadolinium ions from aqueous solution using sonicated emulsion polymer. Int J Innov Res Growth. https://doi.org/10.26671/ijirg.2019.4.8.101
9. Goneam Hamed M, Breky MME, Ghazy O, Borai EH (2022) Separation and preconcentration of cerium (III) and Iron (III) on

magnetic nanocomposite hydrogel. Colloids Surf A Physicochem Eng Aspects 652. https://doi.org/10.1016/j.colsurfa.2022.129779
10. Shahangi Shirazi F, Akhbari K (2016) Sonochemical procedures; The main synthetic method for synthesis of coinage metal ion supramolecular polymer nano structures. Ultrason Sonochem. https://doi.org/10.1016/j.ultsonch.2015.12.003
11. Mahdavian AR, Sehri Y, Salehi-Mobarakeh H (2008) Nanocomposite particles with core-shell morphology II. An investigation into the affecting parameters on preparation of Fe3O4-poly (butyl acrylate-styrene) particles via miniemulsion polymerization. Eur Polym J. https://doi.org/10.1016/j.eurpolymj.2008.05.025
12. Borai EH, Hamed MG (2016) Separation of uranium from rare earth elements using modified polymeric resin. Int J Mater Mech Eng 5(0):19. https://doi.org/10.14355/ijmme.2016.05.003
13. Hamed MG, El-Dessouky SI, Borai EH (2022) Utilization of modified polymeric composite supported crown ether for selective sorption and separation of various beta emitting radionuclides in simulated waste. J Mol Liq 353. https://doi.org/10.1016/j.molliq.2022.118799
14. Borai EH, Hamed MG (2015) Gamma radiation induced preparation of poly (vinylpyrilidone-Maleic acid-Amidoxime) resin for sorption of some metal ions. Proc Int Conf Mater (MATERIALS 2015), pp 238–246
15. Ghazy OA, Khalil SA, Senna MM (2020) Synthesis of montmorillonite/chitosan/ammonium acrylate composite and its potential application in river water flocculation. Int J Biol Macromol. https://doi.org/10.1016/j.ijbiomac.2020.08.022
16. Zhuang S, Wang J (2019) Removal of cobalt ion from aqueous solution using magnetic graphene oxide/chitosan composite. Environ Prog Sustain Energy. https://doi.org/10.1002/ep.12912
17. Parvizi S, Behbahani M, Zeraatpisheh F, Esrafili A (2018) Preconcentration and ultra-trace determination of hexavalent chromium ions using tailor-made polymer nanoparticles coupled with graphite furnace atomic absorption spectrometry: Ultrasonic assisted-dispersive solid-phase extraction. New J Chem 42(12):10357–10365. https://doi.org/10.1039/c8nj01608a
18. Jiang H, Zhang G, Li F, Zhang Y, Lei Y, Xia Y, Jin X, Feng X, Li H (2017) A self-healable and tough nanocomposite hydrogel crosslinked by novel ultrasmall aluminum hydroxide nanoparticles. Nanoscale 9(40):15470–15476. https://doi.org/10.1039/c7nr04722c
19. Ghazy O, Hamed MG, Breky M, Borai EH (2021) Synthesis of magnetic nanoparticles-containing nanocomposite hydrogel and its potential application for simulated radioactive wastewater treatment. Colloids Surf A 621:126613. https://doi.org/10.1016/j.colsurfa.2021.126613
20. Hamed MG, El-kamash AM, El-sayed AA (2021) Selective removal of lead using nanostructured chitosan ion-imprinted polymer grafted with sodium styrene sulphonate and acrylic acid from aqueous solution. Int J Environ Anal Chem 103:5465–5482. https://doi.org/10.1080/03067319.2021.1940158
21. Mencer HJ, Gomzi Z (1994) Swelling kinetics of polymer-solvent systems. Eur Polymer J 30(1):33–36. https://doi.org/10.1016/0014-3057(94)90229-1
22. Shizuka H, Takada K, Morita T (1980) Fluorescence enhancement of dibenzo-18-crown-6 by alkali metal cations. J Phys Chem. https://doi.org/10.1021/j100446a013
23. Weber WJ, Morris JC (1963) Closure to "kinetics of adsorption on carbon from solution." J Sanit Eng Div 89(6):53–55. https://doi.org/10.1061/jsedai.0000467
24. El-Kamash AM, Zaki AA, El Geleel MA (2005) Modeling batch kinetics and thermodynamics of zinc and cadmium ions removal from waste solutions using synthetic zeolite A. J Hazard Mater. https://doi.org/10.1016/j.jhazmat.2005.07.021
25. Hassan HS, El-Kamash AM, Ibrahim HAS (2019) Evaluation of hydroxyapatite/poly(acrylamide-acrylic acid) for sorptive removal of strontium ions from aqueous solution. Environ Sci Pollut Res. https://doi.org/10.1007/s11356-019-05755-1
26. Wang J, Guo X (2020) Adsorption isotherm models: Classification, physical meaning, application and solving method. Chemosphere. https://doi.org/10.1016/j.chemosphere.2020.127279
27. Manohar DM, Noeline BF, Anirudhan TS (2006) Adsorption performance of Al-pillared bentonite clay for the removal of cobalt(II) from aqueous phase. Appl Clay Sci 31(3–4):194–206. https://doi.org/10.1016/j.clay.2005.08.008
28. Bhatnagar A, Minocha AK, Sillanpää M (2010) Adsorptive removal of cobalt from aqueous solution by utilizing lemon peel as biosorbent. Biochem Eng J 48(2):181–186. https://doi.org/10.1016/j.bej.2009.10.005
29. Dobrowolski R, Szcześ A, Czemierska M, Jarosz-Wikołazka A (2017) Studies of cadmium(II), lead(II), nickel(II), cobalt(II) and chromium(VI) sorption on extracellular polymeric substances produced by Rhodococcus opacus and Rhodococcus rhodochrous. Biores Technol 225:113–120. https://doi.org/10.1016/j.biortech.2016.11.040